# SH3 domain-binding glutamic acid-rich protein-like 3 is associated with hyperglycemia and a poor outcome in Epstein-Barr virus-negative gastric carcinoma

HOUQIANG LI[1-3*], LANQING ZHENG[1,4*], XIA ZHANG[1-3], XUNBIN YU[1-3], GUODONG ZHONG[5], XIAOYAN CHEN[1-3], XIN CHEN[1-3] and LINYING CHEN[6]

[1]Shengli Clinical Medical College of Fujian Medical University, Fuzhou, Fujian 350001, P.R. China; [2]Department of Pathology, Fuzhou University Affiliated Provincial Hospital, Fuzhou, Fujian 350001, P.R. China; [3]Department of Pathology, Fujian Provincial Hospital, Fuzhou, Fujian 350001, P.R. China; [4]Nursing Department, Fujian Provincial Hospital, Fuzhou, Fujian 35001, P.R. China [5]Department of Pathology, The Second Affiliated Hospital of Fujian Traditional Chinese Medical University, Fuzhou, Fujian 350003, P.R. China; [6]Department of Pathology, The First Affiliated Hospital of Fujian Medical University, Fuzhou, Fujian 350005, P.R. China

Received June 2, 2024; Accepted September 3, 2024

DOI: 10.3892/ol.2024.14754

**Abstract.** SH3 domain-binding glutamic acid-rich protein-like 3 (SH3BGRL3) is involved in several human cancers. However, its relationship with gastric cancer (GC) remains elusive. Multiple online bioinformatic tools were used to evaluate the messenger (m)RNA expression levels of SH3BGRL3 in GC using data from The Cancer Genome Atlas and Gene Expression Omnibus databases. Reverse transcription-quantitative PCR and tissue microarray-based immunohistochemistry were performed to assess SH3BGRL3 expression in relation to clinicopathological parameters and outcomes in patients with GC. Significant differentially expressed genes (DEGs) of SH3BGRL3 were enriched and visualized. Furthermore, associations between the expression of SH3BGRL3 and the infiltration of immune cells were explored. SH3BGRL3 exhibited aberrant expression in tumor tissues compared with adjacent normal tissues at the mRNA and protein expression levels, especially in Epstein-Barr virus-negative GC (EBVnGC). Higher SH3BGRL3 expression was significantly associated with increasing tumor-node-metastasis staging, tumor budding, perineural invasion, EGFR expression, and a notably higher preoperative blood glucose concentration in clinical specimens. Multivariate analysis revealed that higher SH3BGRL3 expression was an independent adverse prognostic factor for the overall survival of patients with EBVnGC (hazard ratio, 1.666; P=0.018). Furthermore, the stratified analysis revealed that the SH3BGRL3 phenotype could help to refine prognosis in patients. The C-index of the nomogram was 0.740 when combining SH3BGRL3 with other clinicopathological parameters, which indicated a good model for clinical follow-up decisions. Gene functional enrichment analysis also revealed that the DEGs of SH3BGRL3 were mainly enriched in regulating ATP metabolism, ATP synthesis, oxidative phosphorylation and the electron transport chain in GC. Moreover, a higher SH3BGRL3 expression was significantly positively correlated with the infiltrating macrophages in GC. In conclusion, SH3BGRL3 is upregulated in GC, particularly in EBVnGC. Higher SH3BGRL3 expression is closely associated with hyperglycemia and poor outcomes in patients with EBVnGC, suggesting its potential as a biomarker and prognostic predictor.

## Introduction

Gastric cancer (GC) is one of the most common malignant tumors of the digestive system. It is the fifth leading cause of cancer-related deaths and the fourth leading cause of cancer-related morbidity (1). In addition to chronic *Helicobacter pylori* (*H. pylori*) infection, the carcinogenesis and progression of GC involve complex genetic and epigenetic alterations, including chromosomal instability, abnormalities in oncogenes, tumor suppressor genes, several growth factors, DNA repair genes and metabolic disturbances. Based on high throughput sequencing data in The Cancer Genome Atlas (TCGA), GC has been categorized into four molecular subtypes: i) Epstein-Barr virus (EBV)-positive; ii) microsatellite-instable; iii) genomically stable; iv) and chromosomally unstable (2). Although the TCGA molecular subtypes provide a promising application for stratified management and targeted therapy, the prognosis for most patients remains poor. In

*Correspondence to:* Dr Linying Chen, Department of Pathology, The First Affiliated Hospital of Fujian Medical University, 20 Chazhong Road, Taijiang, Fuzhou, Fujian 350005, P.R. China
E-mail: chenly2006@126.com

Dr Xin Chen, Department of Pathology, Fujian Provincial Hospital, 134 East Street, Gulou, Fuzhou, Fujian 350001, P.R. China
E-mail: 786262810@qq.com

*Contributed equally

*Key words:*

contrast to the EBV-positive subtype, which has an abundance of lymphoid stroma that allows for possible immune checkpoint inhibition, most cases of Epstein-Barr virus-negative GC (EBVnGC) lack targeted therapeutic drugs due to tumor heterogeneity (2,3). Thus, finding a potential biomarker for promising effective therapeutic targets will become an essential strategy for GC, especially for EBVnGC.

SH3 domain-binding glutamic acid-rich protein-like3 (SH3BGRL3), also named tumor necrosis factor inhibitory protein 1, belongs to the thioredoxin superfamily, which maps to chromosome 1p34.3-p35 with 279 nucleotides (4). It encoding cytoplasmic protein is 27 kDa, showing a highly similar structure to that of the glutathione peroxidase of *Escherichia coli*, an enzyme with oxidoreductase activity (5). SH3BGRL3 is a highly evolutionarily conserved gene in the early stages of zebrafish embryonic development and diverse organogenesis (6). Previous studies have reported that SH3BGRL3 is upregulated and its expression is closely associated with poor outcomes in certain human malignancies, including urothelial carcinoma, clear cell renal carcinoma and glioblastoma (7-13). In these studies, SH3BGRL3 was reported to interact with the EGFR family, including ErbB1/EGFR and ErbB2/human epidermal growth factor receptor 2 (HER-2) (10-12). Despite this, the role of SH3BGRL3 expression and its clinical significance in GC, particularly in EBVnGC, remains unclear.

The relationship between glucose metabolism, diabetes and the development of GC has been reported in several studies (14-17). Tumor cells rely on glucose for energy supplements, and the status of hyperglycemia contributes to tumor growth through the effects of genetic mutations, epigenetic modification and proteomic alteration (14). Altered glucose metabolism, including aerobic glycolysis and a dysfunctional mitochondrial oxidative phosphorylation (OXPHOS) system, has been recognized as a critical hallmark characteristic of cancer cells (18). In the process of a biochemical reaction, many intermediate metabolic products are released, which could promote tumor growth and induce alterations in immune responses within the tumor microenvironment (TME) (19). It has been reported that *SH3BGRL3* potentiates the functions of several carcinogenic pathways, including PI3K, Akt and Mammalian target of rapamycin (mTOR), all of which are involved in glycolysis in tumor cells (9-11). Nevertheless, whether SH3BGRL3 is involved in glucose metabolism in patients with GC remains elusive. Exploring the relationships between SH3BGRL3 expression and preoperative blood glucose concentration and their possible underlying mechanisms would be beneficial.

The expression of SH3BGRL3 and its associations with clinicopathological parameters and patient outcomes were assessed in the present study to determine its prognostic significance in GC. To determine the messenger (m)RNA level of *SH3BGRL3*, RNA sequencing data obtained from public databases and mRNA detection by reverse transcription (RT)-quantitative (q)PCR on fresh tissues were evaluated. Tissue microarrays (TMA) and immunohistochemistry (IHC) were performed to assess the expression of SH3BGRL3 protein in GC. In addition, a functional enrichment analysis of differentially expressed genes (DEGs) and immune infiltrating cells related to SH3BGRL3 were assessed and visualized.

## Materials and methods

*Data mining from public databases*. Online bioinformatic tools, including the Tumor Immune Estimation Resource 2.0 (TIMER 2.0; http://timer.cistrome.org), the Human Protein Atlas (HPA; proteinatlas.org) and the Gene Expression Profiling Interactive Analysis (GEPIA; http://gepia2.cancer-pku.cn/) databases were used to assess the levels of SH3BGRL3 mRNA in GC tissues and their related normal tissues. $|\log_2$ fold change$|>1$ and a q-value $<0.01$ was considered significant. The Kaplan-Meier plotter (https://kmplot.com/analysis/) was employed for the analysis of the Gene Expression Omnibus (GEO) database (https://www.ncbi.nlm.nih.gov/geo/; including GSE14210, GSE15459, GSE22377, GSE29272, GSE51105 and GSE62254) to investigate the association between SH3BGRL3 expression, overall survival (OS) and post-progression survival (PPS).

To assess the potential functions of SH3BGRL3, the related DEGs were identified from TCGA_STAD RNA-sequencing data using LinkedOmics (http://www.linkedomics.org/), and functional enrichment analysis was performed. Kyoto Encyclopedia of Genes and Genomes (KEGG) pathway and Gene Ontology (GO) analyses, comprising biological process (BP), cellular component (CC) and molecular function (MF), were performed using the top 1,000 DEGs ($|r|>0.3$ and $P<0.05$) with the R package 'cluster profiler' (version 3.0.4; https://bioconductor.org/packages/clusterProfiler/). Gene set enrichment analysis (GSEA) was performed using the Molecular Signatures Database (MSigDB; http://www.gsea-msigdb.org/gsea/msigdb/collections.jsp), according to the median levels of SH3BGRL3 expression, and an enrichment with normalized enrichment score >1 or <-1, and false discovery rate q-value $<0.05$ was considered significant. In addition, GeneMANIA (http://genemania.org/) and Protein-Protein Interaction Networks Functional Enrichment Analysis (STRING; version 11.5; https://cn.string-db.org) were used to evaluate the associated networks of SH3BGRL3. TIMER and Tumor and Immune System Interaction Database (TISIDB; http://cis.hku.hk/), two online web servers, were used to assess the relationships between SH3BGRL3 gene expression and infiltrating immune cells in the TCGA_STAD database. In TIMER and TISIDB, the Estimating the Proportion of Immune and Cancer cells calculation was used to predict the tumor immune score.

*Clinical populations*. A total cohort of 607 consecutive patients from Fujian Provincial Hospital (Fuzhou, China), who were pathologically diagnosed as GC between January 2014 and December 2015, was enrolled. The ages of the patients ranged from 27-89 years, with a median age of 63 years. Two pathologists (HQL and LYC) reviewed original hematoxylin and eosin (H&E) slides and recorded the clinicopathological parameters of the patients from the hospital medical systems. Preoperative blood glucose was also recorded. OS was defined as the duration from the date of initial diagnosis to the date of death. An additional cohort including seven pairs of fresh EBVnGC tissues and their corresponding normal gastric tissues were also collected at Fujian Provincial Hospital (Fuzhou, China) between August 2021 and November 2021. In this cohort, the ratio of men to women was 3:4, with a median

age of 74 years (range, 54-75 years). The inclusion criteria of the aforementioned patient were as follows: i) Pathologically diagnosed with gastric adenocarcinoma; ii) available paired cancer tissues and para-carcinoma tissues; and iii) radical gastrectomy performed. Furthermore, the exclusion criteria were as follows: i) Recurrent or metastatic disease; ii) neoadjuvant therapy administered; iii) mixed adenocarcinoma and neuroendocrine tumors; iv) loss to follow-up; and v) death within 1 month after surgery. The diagnosis and staging were based on the 5th edition of the World Health Organization (WHO) classification and staging of tumors of the digestive system: Gastric tumors (20).

*Assessment of tumor budding (BUD).* Similarly, two pathologists assessed the status of BUD according to the guidelines of the International Tumor Budding Consensus Conference (21). Microscopically, a single tumor cell or a cell cluster of ≤4 tumor cells in the invasive front area was identified as a BUD. BUD was assessed in the 'hot spot' region at a x200 high power field (Leica light microscope DM3000; Leica Microsystems GmbH), which was converted to standardized numbers every 0.785 $mm^2$. BUD was classified as the following: Bd1, 0-4 buds; Bd2, 5-9 buds; and Bd3, ≥10 buds. Based on the results, cases were graded as budding low (Bd1) and budding high (Bd2/3). A consensus review using a multi-head microscope was performed when inconsistencies arose.

*TMA construction.* A TMA was constructed for IHC staining (Fig. S1A). For the donor formalin-fixed paraffin-embedded (FFPE) tissues fixed with 10% neutral formalin (PH 7.2-7.4; room temperature for 18 h), the representative regions of each H&E-stained slide were labeled (Fig. S1B), including the GC tumor and the paired adjacent normal gastric tissues. Cores with a 1.5-mm diameter at each corresponding area were taken and transferred into the 'recipient' paraffin blocks by punching tissue cylinders. The resulting array had nine cores across (x-axis) and seven cores down (y-axis). Unstained 4-$\mu$m sections of the TMA were prepared and then adhered to SuperFrostPlus™ glass slides (Matsunami Glass Ind., Ltd.). For every tissue array block, one slide was stained with H&E to confirm the presence of representative tumors. The TMA slides were stained with H&E using the HistoCore SPECTRA Workstation (Leica Biosystems GmbH) according to a preset program. The TMAs were placed on the burner at 70˚C for 30 min and then sequentially went through the steps of dewaxing, dehydration, hematoxylin staining, differentiation, bluing, eosin staining, dehydration, clearing and cover-slipping (Table SI).

*IHC staining and scoring.* For the IHC of SH3BGRL3, TMA sections were incubated overnight at 4˚C with a 1:500 dilution of rabbit SH3BGRL3 antibodies (cat. no. HPA030848; Sigma-Aldrich; Merck KGaA), followed by secondary antibodies and DAB. IHC was performed as described previously (13). The SH3BGRL3 immunostaining was assessed microscopically, and ≥3 high power fields (Leica light microscope DM3000; x200) in hotspot areas were imaged, respectively. According to the operating instructions and the ImageJ software (https://imagej.nih.gov/ij/index.html; version 1.53 h), the intensity of SH3BGRL3 staining was calculated and represented with an average optical density (AOD). The optimal cut-off value of the SH3BGRL3 expression was calculated by the R package 'survminer'.

The TMA slides were also stained with the following antibodies: MutL protein homolog 1 (MLH1) (cat. no. MX063), postmeiotic segregation increased 2 (PMS2) (cat. no. EP51), MutS homolog (MSH)2 (cat. no. MX061), MSH6 (cat. no. MX056) and EGFR (cat. no. SP111), using the Lumatas platform (Fuzhou Maixin Biotechnology Development Co., Ltd.). The IHC automated staining protocol was performed according to the manufacturer's instructions. In brief, after being deparaffinized in dewaxing fluid at 50˚C for 5 min, the 4-$\mu$m sections of the TMA were treated with Max2inOneTM LP (Fuzhou Maixin Biotechnology Development Co., Ltd.) at 99˚C for 20 min. The samples were cooled to room temperature, washed three times with PBS, blocked with 3% $H_2O_2$ at 32˚C for 10 min and washed with PBS twice. The primary antibodies were added to the section and the section was incubated at 32˚C for 30 min. After final washing with PBS twice, pre-diluted HRP-Polymer Goat Anti-Rabbit or Mouse IgG (cat. no. TT0801, Fuzhou Maixin Biotechnology Development Co., Ltd.) was dropped onto the slices and the slices were incubated for 10 min at 32˚C, and then washed with PBS twice. The DAB detection kit chromogenic liquid was added to the sections for 5 min and then stopped with PBS twice. After washing with water twice, the section was redyed with hematoxylin for 25 sec at 26˚C, followed by PBS for 30 sec. The slices were dehydrated using a series of concentrations of ethyl alcohol and treated with xylene for 3 min at room temperature. Finally, the sections were sealed with neutral gum and observed under a microscope. HER-2 (cat. no. 4B5) staining was performed on 4-$\mu$m sections cut from the FFPE blocks using a Benchmark ULTRA immunostainer (Roche Tissue Diagnostics). The HER-2 IHC automated staining protocol was performed as described previously (22). The details of antibodies, incubation conditions and antigen retrieval are listed in Table SII. PBS was used as the negative control.

EGFR staining was characterized as membranous and/or cytoplasmic. EGFR staining was assessed as 0, 1, 2 or 3 according to the recommendations in previous literature (23): 0, negative or weak staining in <10% of tumor cells; 1+, weak staining in >10% of tumor cells; 2+, moderate staining in >10% of tumor cells; and 3+, intense staining in >10% of tumor cells (Fig. S2). Tumors classified as 3+ were considered to have high EGFR expression. HER-2 immunostaining (Fig. S1C) was scored according to the American Society of Clinical Oncology (ASCO) guidelines (24). The four mismatch repair (MMR) proteins, including MLH1, PMS2, MSH2 and MSH6, showed nuclear staining, which were classified as proficient (p)MMR (no loss of MMR proteins) or defective (d)MMR (≥1 losses of MMR proteins) (25). Immunohistochemical staining was observed under a Leica light microscope DM3000 (Leica Microsystems GmbH).

*In situ hybridization (ISH) and fluorescence ISH (FISH).* Unstained 4-$\mu$m sections of FFPE tissue fixed with 10% neutral formalin (pH 7.2-7.4; 26˚C) were prepared for the ISH and FISH assays. The ISH assay was performed with EBV-encoded small RNA (EBER) probe (cat. no. PB0589; Leica Biosystems GmbH) using an automatic staining

device (Bond-III; Leica Biosystems GmbH). The EBER-ISH automated staining protocol was performed according to the manufacturer's instructions as previously described (26). In brief, slides were automatically deparaffinized three times at 72˚C for 1 min with BondDewax (cat. no. AR9222, Leica Biosystems GmbH), rinsed with gradient alcohols and four times with BOND Wash (cat. no. AR9590-CN; Leica Biosystems GmbH) at room temperature. After incubation with enzyme proteinase K (cat. no. RE7160-k; Leica Biosystems GmbH) for 15 min at 37˚C. The Ready-to-Use EBER probe (containing formamide) was applied for the slides and incubated at 26˚C for 2 h. After blocked with 3% $H_2O_2$ at 26˚C for 5 min, the slides were incubated with BOND Ready-to-Use Anti-Fluorescein Antibody (cat. no. AR0222; Leica Biosystems GmbH) for 15 min, post-primary reagent for 8 min and polymer for 8 min (all at 26˚C), with four times BOND Wash rinses between steps, 3-5 sec each time. After the final polymer incubation, slides were rinsed twice with BOND Wash and once with distilled water. Staining was performed with DAB for 10 min at 26˚C, followed by rinsing in distilled water, hematoxylin counterstaining for 25 sec at 26˚C, rinsing in BOND Wash and distilled water at 26˚C and cover-slipping. The results of the ISH assay were observed under a Leica light microscope DM3000 (Leica Microsystems GmbH). The brown nuclear staining was considered positive. The known EBER-positive nasopharyngeal carcinoma tissues were used as the positive control, and a sense probe for EBER was used as the negative control.

The FISH assay was performed with PathVysion HER-2 DNA Probe Kit II (Abbott Pharmaceutical Co., Ltd.). All the experimental operations were carried out according to the manufacturer's instructions. In summary, prior to hybridization, slices were deparaffinized with xylene twice for 10 min each and hydration with ethyl alcohol (100, 95 and 75%) and distilled water, all 5 min at room temperature. Following these, sections were boiling in distilled water for 20 min and cooled to room temperature. Subsequently, the sections were treated with enzyme proteinase K (cat. no. 03L7860; Abbott Pharmaceutical Co., Ltd.) at 37˚C for 10 min, and then washed with 2x SSC solution for 1 min at room temperature. After that, the slices underwent dehydration with gradient alcohols (100, 95 and 75%, all 3 min) at room temperature. Then the PathVysion HER-2 DNA Probe Kit II was applied before denaturation at 75˚C for 5 min and hybridization at 37˚C for After 14 h, the slides were washed with NP-40 (0.3%, pH 7.0-7.5) at 72˚C for two min to remove any unbound probes and counterstained with DAPI at room temperature for 10 min. PathVysion HER-2 DNA Probe kit II consists of two labeled DNA probes. The LSI HER-2/neu probe that spans the HER2 gene (17q11.2-12) is labeled in SpectrumOrange, while the CEP17 probe is labeled in SpectrumGreen and hybridizes to the alpha satellite DNA located at the centromere of chromosome 17 (17p11.1-q11.1). Inclusion of the CEP17 probe allows detection of the relative copy number of the HER2 gene. FISH signals were assessed using an Olympus fluorescence microscope BX63 (Olympus Corporation; objective lens, x100), and the results were assessed using the methods described in the ASCO guidelines (24). The total numbers of HER2 and CEP17 signals were counted in 20 adjacent interphase tumor cell nuclei, using a fluorescence microscope and appropriate filters. The ratios of HER2 signals to CEP17 signals were calculated regardless of IHC status as follows: When the ratio was <1.8, the gene was considered non-amplified, and when it was >2.2, the gene was considered to be amplified. If the ratio was within the range of 1.8 to 2.2 at the initial count, an additional 20 tumor cells were counted. If the final ratio for 40 nuclei was 2.0 or higher, the case was deemed to have HER2 amplification (Fig. S1D).

*RT-qPCR*. Total RNA was extracted using TRIzol™ reagent (Takara Bio, Inc.). The cDNA was synthesized using the PrimeScript™ RT Reagent Kit (cat. no. RR037; Takara Bio, Inc.). Subsequently, cDNA was obtained following the completion of reverse transcription at 37˚C for 15 min and 85˚C for 5 sec, during which time the enzyme was inactivated. qPCR reactions were performed using TB Green (cat. no. RR820; Takara Bio, Inc.) using the LightCycler® 480 Real-Time PCR System (Roche Diagnostics). The reaction conditions were as follows: Pre-denaturation at 95˚C for 30 sec, followed by 95˚C for 5 sec and 60˚C for 34 sec, 45 cycles; melting reaction at 95˚C for 15 sec, 60˚C for 1 min and 95˚C for 15 sec, 1 cycle. The relative SH3BGRL3 mRNA expression was calculated using the $2^{-\Delta\Delta Cq}$ method (27). All the experimental operations were carried out according to the manufacturer's instructions. The sequences of the primers used are as follows: SH3BGRL3 (forward), 5'-CCACCCCAGATTGTCAACGG-3'; SH3BGRL3 (reverse), 5'-TCAAGCCAGCTTCAGGAACTC-3'; GAPDH (forward), 5'-GGTGTGAACCATGAGAAGTATGA-3'; and GAPDH (reverse), 5'-GAGTCCTTCCACGATACCAAAG-3'.

*Statistical analysis*. Graphs were generated and statistical analysis was performed using GraphPad Prism 9.0 (Dotmatics), RStudio (V1.4.110) software (http://www.r-project.org/) and SPSS Statistics 26.0 (IBM Corp.), respectively. An unpaired t-test was employed for the analysis of SH3BGRL3 expression utilizing the GEPIA database and TIMER database, and the AOD of SH3BGRL3 staining. The expression of SH3BGRL3 mRNA in the local datasets was analyzed using a paired t-test. The correlation between SH3BGRL3 expression and clinicopathological parameters was evaluated using Pearson's $\chi^2$ test. A log-rank test was performed to perform survival analysis, and RStudio generated Kaplan-Meier curves. Univariate and multivariate Cox regression analyses were performed to analyze the prognostic variables associated with OS. A nomogram was generated by RStudio based on the results of the multivariate Cox regression analysis. Moreover, the predictive ability was evaluated with the concordance index (C-index), and calibration plots were generated to compare the predicted probability of OS with the observed outcome. $P<0.05$ was considered to indicate a statistically significant difference.

## Results

*SH3BGRL3 is upregulated and associated with poor prognosis in GC in analysis of public databases*. A comprehensive analysis of SH3BGRL3 expression in normal human tissue and cancers was conducted using data from the HPA and GEPIA. The results demonstrated that SH3BGRL3 was widely distributed in human tissues and cancers (Fig. S3). The datasets

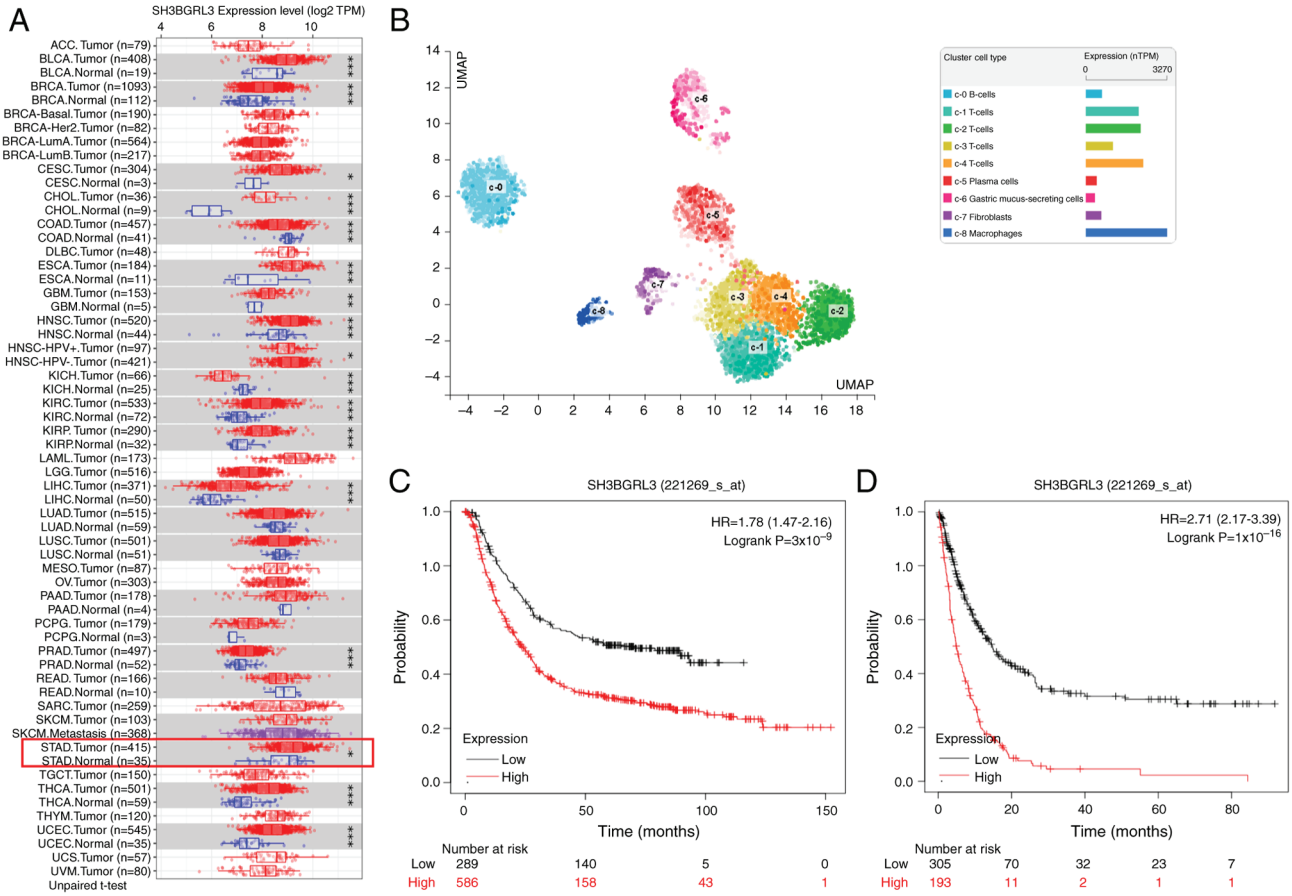


Figure 1. Expression and prognosis analyses of SH3BGRL3 in GC using different databases. (A) The Tumor Immune Estimation Resource revealed that SH3BGRL3 was remarkably aberrant and expressed in several human cancers, including GC. (B) Single-cell analysis demonstrated that SH3BGRL3 was weakly expressed in normal gastric epithelial cells. Kaplan-Meier plotters revealed that SH3BGRL3 expression was significantly associated with (C) overall survival and (D) post-progression survival in GC. *P<0.05, **P<0.01, ***P<0.001, unpaired t-test. SH3BGRL3, SH3 domain-binding glutamic acid-rich protein-like 3; GC, gastric cancer; TPM, transcripts per million; nTPM, number of TPM; UMAP, uniform manifold approximation and projection; HR, hazard ratio; CI, confidence interval.

from TIMER, a data analysis platform, were analyzed with 415 TCGA_STAD and 35 corresponding normal samples. The results revealed that SH3BGRL3 was significantly upregulated in multiple malignancies compared with the corresponding normal tissues, including GC (P<0.05; Fig. 1A). Moreover, single-cell analysis from the HPA revealed that SH3BGRL3 was weakly expressed in normal gastric mucus-secreting cells, which was lower than that in immune cells and muscle fiber cells (Fig. 1B).

Subsequently, the effect of SH3BGRL3 expression on GC prognosis was assessed using the GEO database. A total of 875 and 498 GC samples were used to analyze the association between SH3BGRL3 expression and OS and PPS, respectively. Kaplan-Meier plots demonstrated that a high expression of SH3BGRL3 was significantly associated with poor OS (P<0.0001; Fig. 1C) and PPS (P<0.0001; Fig. 1D) in patients with GC. Patients with high SH3BGRL3 expression were 1.78 times more likely to die than patients with low expression. The median time of OS was 23.6 months for the high SH3BGRL3 group and 70.2 months for the low expression group. Parallel to the OS results, patients with high SH3BGRL3 expression had a 2.71-fold higher risk of relapse than those with low expression. In the high SH3BGRL3 group, the median time for PPS was 4.9 months, whilst in the low expression group, the median time was 14.8 months.

Furthermore, the stratified analysis revealed that patients with GC with the characteristics of pathological tumor-node-metastasis (pTNM) stage III, pTNM stage IV, lymph node involvement, intestinal histological type, male sex and no HER-2 amplification, could be divided into groups with different outcomes based on SH3BGRL3 expression. Cases with low SH3BGRL3 expression had significantly longer OS compared with those with high expression (Fig. S4). This suggests that a high expression of SH3BGRL3 is an adverse factor for the outcomes of patients with GC.

*High SH3BGRL3 expression is associated with high preoperative blood glucose concentration and aggressive clinicopathological characteristics in patients with EBVnGC.* As that the mRNA level of SH3BGRL3 was upregulated in GC, the present study subsequently assessed SH3BGRL3 protein expression in GC. First, TMA-based immunostaining was used to detect SH3BGRL3 protein expression in nonselective GC and adjacent normal gastric tissues (Fig. 2). There was weak or negative staining of SH3BGRL3 protein in normal gastric epithelial cells, similar to the results of single-cell sequencing (Fig. 2A). By contrast, there was

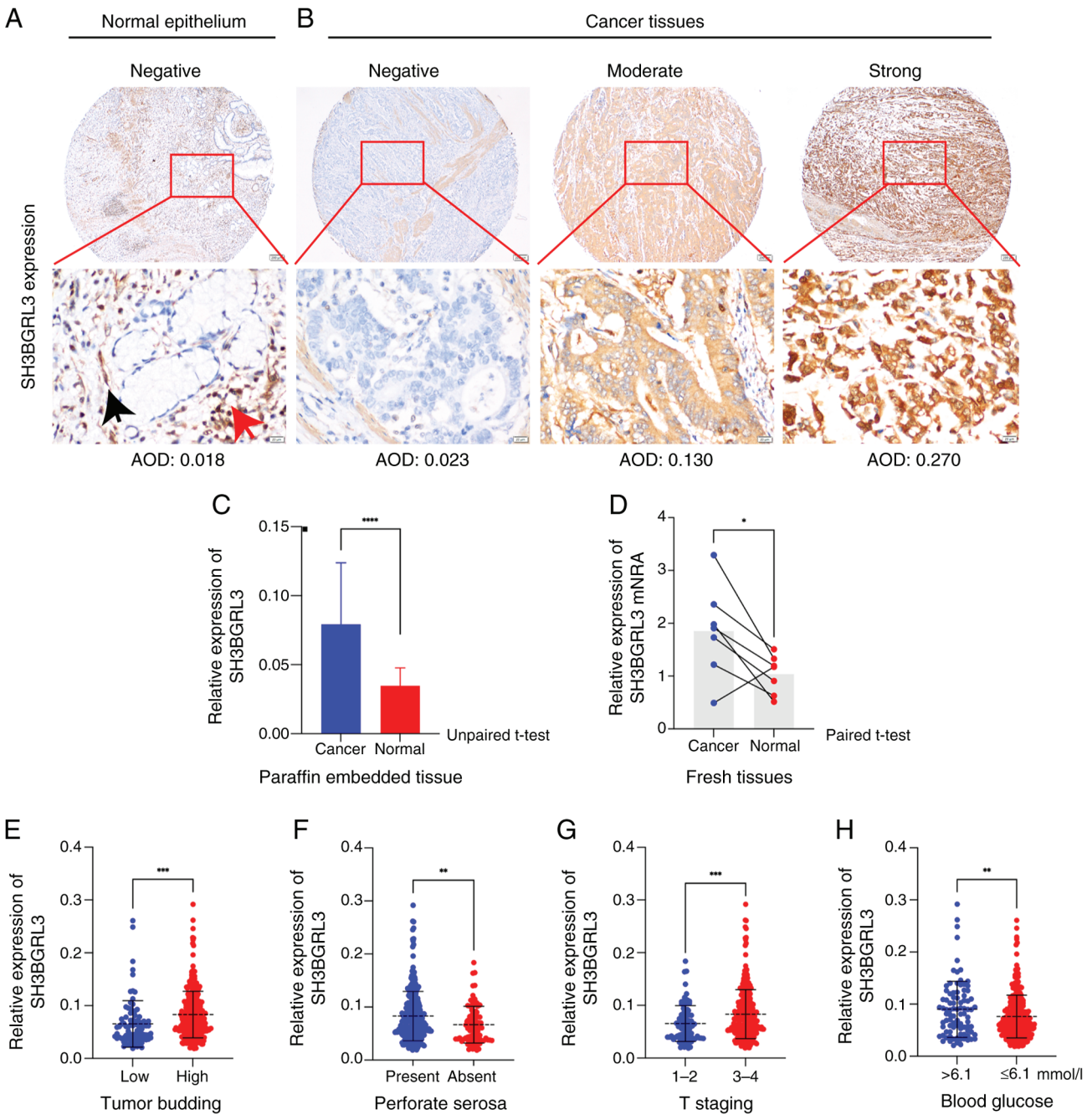


Figure 2. Expression analysis of SH3BGRL3 in Epstein-Barr virus-negative gastric cancer. Representative images of (A) normal gastric tissues (original magnification, x20 and x400) and (B) the different SH3BGRL3 expression in GC tumor tissues (original magnification, x20 and x400). The AOD values are the specific values for the representative images. SH3BGRL3 (C) protein and (D) mRNA expression was higher in GC tissue than that of normal gastric tissues. SH3BGRL3 expression was significantly higher in patients with GC with (E) higher tumor budding, (F) presence of perforate serosa, (G) higher T stage and (H) blood glucose level of >6.1 mmol/l. $^{*}$P<0.05; $^{**}$P<0.01; $^{***}$P<0.001; $^{****}$P<0.0001. SH3BGRL3, SH3 domain-binding glutamic acid-rich protein-like 3; T, tumor; AOD, average optical density.

stronger staining in the cytoplasm of the lymphocytes and muscle fibrocytes (Figs. 2A and S5C) and GC cells (Figs. 2B and S5C). Subsequently, due to the abundant lymphoid stroma in EBV-positive gastric cancers (Fig. S5A and B), the present study evaluated the role of SH3BGRL3 in EBVnGC. An ISH assay of EBER was performed, and the EBV-negative cases were selected for further analysis. Finally, 398 patients with EBVnGC with complete clinicopathological and follow-up data were enrolled, including 287 (72.1%) males and 111 (27.9%) females (Table I). The male-to-female ratio was 2.5:1, and the age ranged from 27-89 years, with a median age of 63. Of the 398 patients, 201 died, and the average follow-up time was 45.58 months (ranging from 1-87 months).

For SH3BGRL3 expression, the mean AOD of normal gastric epithelial cells was 0.0348±0.0129 (range, 0.017-0.071; Fig. 2A). Furthermore, the mean AOD of SH3BGRL3 staining in GC tissues was 0.0792±0.0445 (range, 0.019-0.292; Fig. 2B), which was significantly higher than that in normal gastric epithelial cells (P<0.0001; Fig. 2C). The mRNA level of SH3BGRL3 was also demonstrated to be significantly

Table I. Association between SH3 domain-binding glutamic acid-rich protein-like 3 expression and clinicopathological features in patients with Epstein-Barr virus-negative gastric cancer.

| | | SH3BGRL3 expression | | |
|---|---|---|---|---|
| Parameter | Total (n=398) | High (n=313) | Low (n=85) | P-value |
| Sex | | | | 0.3700 |
| Male | 287 | 229 | 58 | |
| Female | 111 | 84 | 27 | |
| Age | | | | 0.5600 |
| >65 years | 152 | 118 | 34 | |
| ≤65 years | 246 | 195 | 51 | |
| Tumor location | | | | 0.8690 |
| Body and cardia | 231 | 181 | 50 | |
| Antrum | 167 | 132 | 35 | |
| Perforate serosa | | | | <0.0001 |
| Presence | 304 | 255 | 49 | |
| Absence | 94 | 58 | 36 | |
| WHO grading | | | | 0.8620 |
| G1-2 | 201 | 158 | 43 | |
| G3 | 197 | 155 | 42 | |
| T staging | | | | <0.0001 |
| T1-T2 | 92 | 56 | 36 | |
| T3-T4 | 306 | 257 | 49 | |
| N staging | | | | 0.0080 |
| N0 | 117 | 79 | 38 | |
| N1-3 | 291 | 244 | 47 | |
| pTNM staging | | | | 0.0010 |
| I-II | 153 | 107 | 46 | |
| III-IV | 245 | 206 | 39 | |
| Cancer embolus | | | | 0.0030 |
| Presence | 105 | 72 | 33 | |
| Absence | 293 | 241 | 52 | |
| Perineural invasion | | | | <0.001 |
| Presence | 182 | 129 | 53 | |
| Absence | 216 | 184 | 32 | |
| BUD | | | | <0.0001 |
| BUD-L | 88 | 53 | 35 | |
| BUD-H | 310 | 260 | 50 | |
| Lauren type | | | | 0.4610 |
| IGC | 235 | 187 | 48 | |
| nIGC | 163 | 126 | 37 | |
| MMR | | | | 0.3970 |
| dMMR | 87 | 67 | 20 | |
| pMMR | 311 | 246 | 65 | |
| HER-2[a] amplification | | | | 0.2800 |
| Positive | 44 | 37 | 7 | |
| Negative | 334 | 260 | 74 | |
| EGFR expression | | | | 0.0130 |
| High | 37 | 35 | 2 | |
| Low | 361 | 278 | 83 | |

[a]n=378. SH3BGRL3, SH3 domain-binding glutamic acid-rich protein-like 3; WHO, World Health Organization; T, tumor; N, node; pTNM, pathological tumor-node-metastasis; BUD, tumor budding; BUD-H, BUD-high; BUD-L, BUD-low, IGC, intestinal gastric cancer, nIGC, non-IGC; MMR, mismatch repair; dMMR, defective MMR; pMMR, proficient mismatch repair; HER-2, human epidermal growth factor receptor 2.

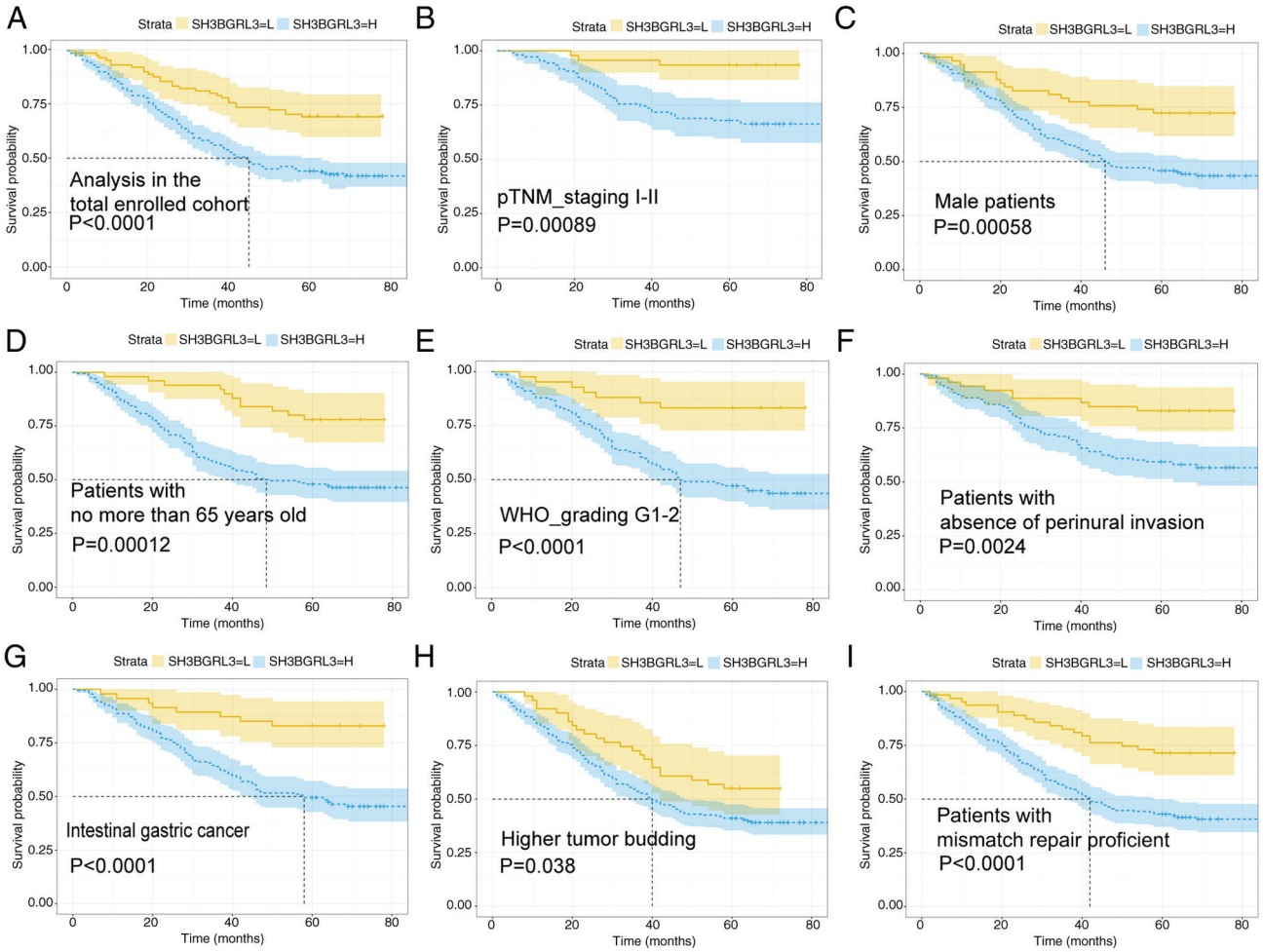


Figure 3. Kaplan-Meier survival analysis of overall survival according to SH3BGRL3 expression in patients with Epstein-Barr virus-negative gastric cancer. Survival analysis in the following subgroups: (A) total enrolled cohort; (B) pTNM stage 1-2; (C) male sex; (D) aged ≤65 years; (E) WHO grade G1-2; (F) absence of perineural invasion; (G) intestinal gastric cancer; (H) higher tumor budding; and (I) proficient mismatch repair. SH3BGRL3, SH3 domain-binding glutamic acid-rich protein-like 3; pTNM, pathological tumor-node-metastasis; WHO, World Health Organization; G, grade; SH3BGRL3-H, SH3BGRL3 high expression; SH3BGRL3-L, SH3BGRL3 low expression.

upregulated in the EBVnGC tissues compared with that in its corresponding normal tissues (P=0.039; Fig. 2D and Table SIII). Moreover, high SH3BGRL3 expression was strongly significantly associated with higher BUD (P=0.001; Fig. 2E), the presence of perforate serosa (P=0.0021; Fig. 2F), a higher tumor (T) stage (P=0.0008; Fig. 2G) and a blood glucose level of >6.1 mmol/l (P=0.0096; Fig. 2H) compared with low SH3BGRL3 expression.

*High SH3BGRL3 expression is an independent adverse prognostic factor in patients with EBVnGC*. To further assess the role of SH3BGRL3 in EBVnGC, the present study dichotomized the SH3BGRL3 expression into high or low groups (cut-off=0.0467, calculated using RStudio software). The results demonstrated that 313 cases had high expression and 85 cases had low expression. In comparison with low expression, high SH3BGRL3 expression was significantly associated with the presence of tumor perforate serosa (P<0.0001), perineural invasion (P<0.001), lymphovascular embolus (P<0.01), pathological T stage (P<0.0001), pathological node stage (P<0.01), pTNM stage (P<0.001) and high BUD (P<0.0001). In addition, high SH3BGRL3 expression was significantly associated with higher EGFR expression, in comparison with low SH3BGRL3 expression (P=0.013; Table I).

Subsequently, the associations between SH3BGRL3 protein expression and outcomes in patients with EBVnGC were analyzed. Kaplan Meier analysis indicated that SH3BGRL3 expression was an influential prognostic factor in patients with EBVnGC. Patients with EBVnGC with high SH3BGRL3 expression demonstrated worse outcomes for OS compared with those with low expression (Logrank=15.085; P<0.0001; Fig. 3A). Furthermore, subgroup analysis suggested that, compared with patients with EBVnGC with low expression, patients with high SH3BGRL3 expression had a worse OS rate in the following subgroups: TNM I-II stage (Logrank=11.037; P<0.001; Fig. 3B), male sex (Logrank=11.459; P<0.001; Fig. 3C), aged ≤65 years (Logrank=14.352; P<0.001; Fig. 3D), WHO grade 1-2 (Logrank=15.222; P<0.0001; Fig. 3E), absence of perineural invasion (Logrank=9.231; P<0.01; Fig. 3F), Lauren intestinal type (20) (Logrank=15.517; P<0.0001; Fig. 3G), high BUD (Logrank=4.099; P=0.038; Fig. 3H) and proficient mismatch repair status (Logrank=15.240; P<0.0001; Fig. 3I). Additionally, multivariate Cox analysis demonstrated that SH3BGRL3 expression was an independent prognostic factor

Table II. Univariate and multivariate analysis of prognostic factors in patients with Epstein-Barr virus-negative gastric cancer.

| | Univariate analysis | | Multivariate analysis | |
|---|---|---|---|---|
| Parameter | HR (95% CI) | P-value | HR (95% CI) | P-value |
| Age (>65 vs. ≤65 years) | 1.363 (1.031-1.802) | 0.0300 | 1.269 (0.950-1.697) | 0.107 |
| Sex (Male vs. female) | 0.923 (0.680-1.252) | 0.6060 | NA | NA |
| Tumor location (Body and cardia vs. antrum) | 1.171 (0.882-1.554) | 0.2740 | NA | NA |
| WHO grading (G3 vs. G1-2) | 1.285 (0.973-1.692) | 0.0780 | 1.480 (0.987-2.219) | 0.058 |
| Lauren types (IGC vs. nIGC) | 0.674 (0.511-0.889) | 0.0050 | 0.662 (0.442-0.991) | 0.038 |
| Perineural invasion (Presence vs. absence) | 2.233 (1.730-3.146) | <0.0001 | 1.534 (1.118-2.106) | 0.008 |
| Cancer embolus (Presence vs. absence) | 3.676 (2.398-5.637) | <0.0001 | 1.741 (1.030-2.943) | 0.038 |
| Perforate serosa (Presence vs. absence) | 3.519 (2.238-5.533) | <0.0001 | 1.387 (0.394-4.878) | 0.610 |
| T staging (T3-4 vs. T1-2) | 3.632 (2.287-5.767) | <0.0001 | 1.019 (0.291-3.832) | 0.977 |
| N staging (N1-3 vs. N0) | 2.923 (2.054-4.164) | <0.0001 | 1.088 (0.660-1.794) | 0.742 |
| pTNM staging (III-IV vs. I-II) | 3.629 (2.555-5.154) | <0.0001 | 2.953 (1.326-3.179) | <0.001 |
| BUD (BUD-H vs. BUD-L) | 2.897 (1.859-4.513) | <0.0001 | 1.840 (1.145-2.958) | 0.012 |
| SH3BGRL3 expression (High vs. low) | 2.228 (1.475-3.366) | <0.0001 | 1.666 (1.093-2.541) | 0.018 |
| Blood glucose (>6.1 vs. ≤6.1 mmol/l) | 1.572 (1.155-2.141) | 0.0040 | 1.515 (1.109-2.069) | 0.009 |

HR, hazard ratio; CI, confidence interval; WHO, World Health Organization; IGC, intestinal gastric cancer; nIGC, non-IGC; T, tumor; N, node; pTNM, pathological tumor-node-metastasis; BUD, tumor budding; BUD-H, BUD-high; BUD-L, BUD-low; SH3BGRL3, SH3 domain-binding glutamic acid-rich protein-like 3; NA, not available.

in patients with EBVnGC. Patients with high SH3BGRL3 expression had an increased risk of death compared with those with low SH3BGRL3 phenotype [hazard ratio (HR), 1.666; 95% confidence interval (CI), 1.093-2.541; P=0.018; Table II].

Subsequently, a prognostic nomogram was constructed to predict the 3- and 5-year survival probabilities in patients with EBVnGC, including the parameters where P<0.1 in the results of multivariate cox regression analysis using the backward method. Finally, a nomogram integrated eight factors, including WHO grading (HR, 1.480; P=0.058), Lauren types (HR, 0.662; P=0.038), perineural invasion (HR=1.534; P=0.008), cancer embolus (HR, 1.741; P=0.038), pTNM stage (HR, 2.953; P<0.001), BUD (HR, 1.840; P=0.012), blood preoperative glucose level (HR, 1.515; P=0.009) and SH3BGRL3 expression (HR, 1.666; P=0.018; Table II and Fig. 4A). The results revealed that the predictive accuracy of the nomogram was good, with a C-index of 0.740 (95% CI, 0.706-0.773). The calibration curves for the 3- and 5-year survival prediction indicated a good accuracy and consistency between predicted probabilities and actual observations (Fig. 4B and C). These results suggest that the nomogram has good discriminative ability and reliability for predicting prognosis.

*DEGs of SH3BGRL3 and associated pathways in GC*. The present study used the DEGs of SH3BGRL3 to analyze and visualize the possible underlying mechanisms of SH3BGRL3 in GC. LinkedOmics revealed that a total of 4,403 genes (dark red dots) were significantly positively correlated with SH3BGRL3, whilst 7,101 genes (dark green dots) were significantly negatively correlated with SH3BGRL3 (Fig. 5A). The top 10 positively correlated genes identified were *GNG5*, *NOP10*, *ZNF593*, *RHOG*, *RNASEK*, *VAMP8*, *TMSB0*, *PFN1*, *CAPZB* and *CLTB* (Fig. 5B). Meanwhile, the top 10 negatively correlated genes identified were *ZNF192*, *TTC21B*, *CELF1*, *ZBTB26*, *ADNP*, *ZNF445*, *FAM168B*, *KLHL15*, *ASH1L* and *NEU3* (Fig. 5C).

A GO and KEGG pathway analysis was performed using RStudio software to evaluate the biological function and molecular mechanism of SH3BGRL3-associated genes. The top 1,000 positively and negatively correlated DEGs were selected for GO and KEGG pathway analysis. In the GO analysis, BP terms were implicated in ATP metabolism processes, the electron transport chain and OXPHOS. CC terms were implicated in mitochondrial protein-containing complexes, ribosomes and ribosomal subunits. Moreover, it was demonstrated that MF terms serves a significant role in transcription coregulator activities, ribosome structural components and electron transfer activities (Fig. 5D). The KEGG pathway analysis indicated the SH3BGRL3-related signaling pathways were enriched in multiple neurodegenerative diseases, ribosome, diabetic cardiomyopathy, OXPHOS, coronavirus disease 2019, colorectal cancer and the proteasome (Fig. 5E). Furthermore, the related interactive networks of SH3BGRL3 were predicted by the online servers of STRING (Fig. 5F) and GeneMANIA (Fig. 5G). It was demonstrated that SH3BGRL3 protein and mRNA were co-expressed and physically interacted with ErbB1/EGFR and ErbB2/HER-2.

To further assess the possible biological pathways enriched by SH3BGRL3 expression, the present study performed GSEA between the SH3BGRL3 low-expression group and high-expression group based on the TCGA_STAD and MSigDB datasets. Based on the main results, the high-expression group had significantly more positive regulatory gene sets for OXPHOS and proteasome than the low-expression group

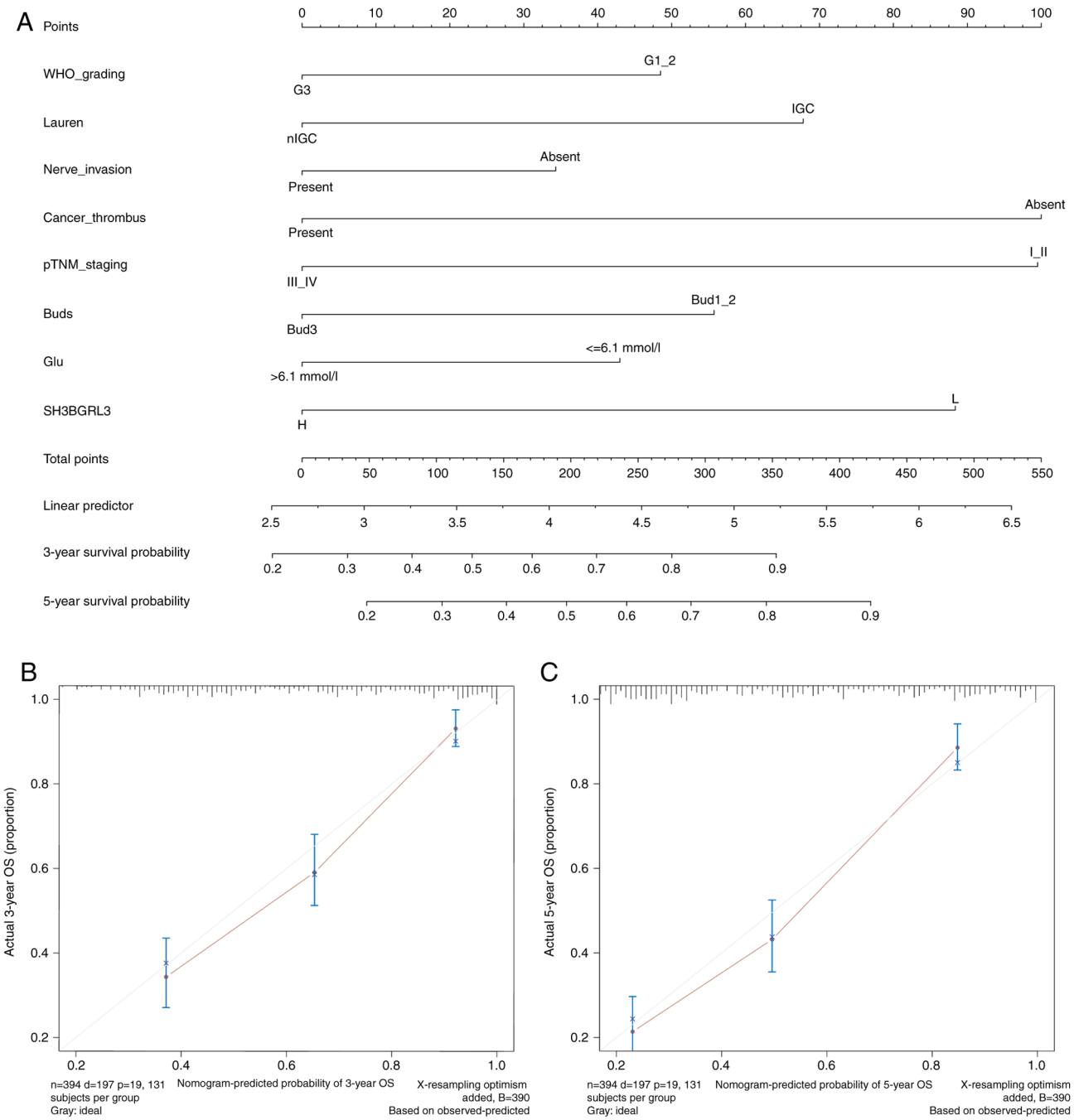


Figure 4. Nomogram for predicting the prognosis of patients with EBVnGC. (A) Nomogram predicting the 3-year and 5-year OS of patients with EBVnGC, including the parameters of WHO grading, Lauren types, perineural invasion, tumor embolus, pTNM staging, tumor budding, blood glucose level and SH3BGRL3 expression. The total score was calculated by adding the scores corresponding to each variable, and the total scores predicted the 3-year or 5-year survival probability of a patient to the lowest survival rate scale. Nomogram calibration for (B) 3-year and (C) 5-year OS. EBVnGC, Epstein-Barr virus-negative gastric cancer; OS, overall survival; WHO, World Health Organization; pTNM, pathological tumor-node-metastasis; SH3BGRL3, SH3 domain-binding glutamic acid-rich protein-like 3; IGC, intestinal gastric cancer; nIGC, non-IGC; Bud, tumor budding; Glu, glucose level.

(Fig. 6A and B). In contrast, the negative regulatory gene sets of lysine degradation (Fig. 6C), the insulin signaling pathway (Fig. 6D), ATP synthase (ATP)-binding cassette transporters (Fig. 6E) and the mTOR signaling pathway (Fig. 6F) were significantly enriched in the low-expression group, in comparison with the high-expression group.

*Correlation of SH3BGRL3 expression with immune cell infiltration*. The results of TIMER analysis revealed that high SH3BGRL3 expression was positively correlated with more macrophages (P<0.001) and natural killer (NK; P<0.0001) infiltrating cells but negatively correlated with $CD4^+$ T (P<0.001) and $CD8^+$ T (P<0.001) infiltrating cells (Fig. 7A). The results of TISIDB analysis demonstrated that the expression of SH3BGRL3 widely affected the infiltrating immune cells within TME in 28 types of malignant tumors (Fig. 7B). Further analysis revealed significant positive correlations between SH3BGRL3 expression and infiltrating macrophages, activated dendritic cells, NK-$CD56^{dim}$ subgroups and monocytes (P<0.0001; Fig. 7C).

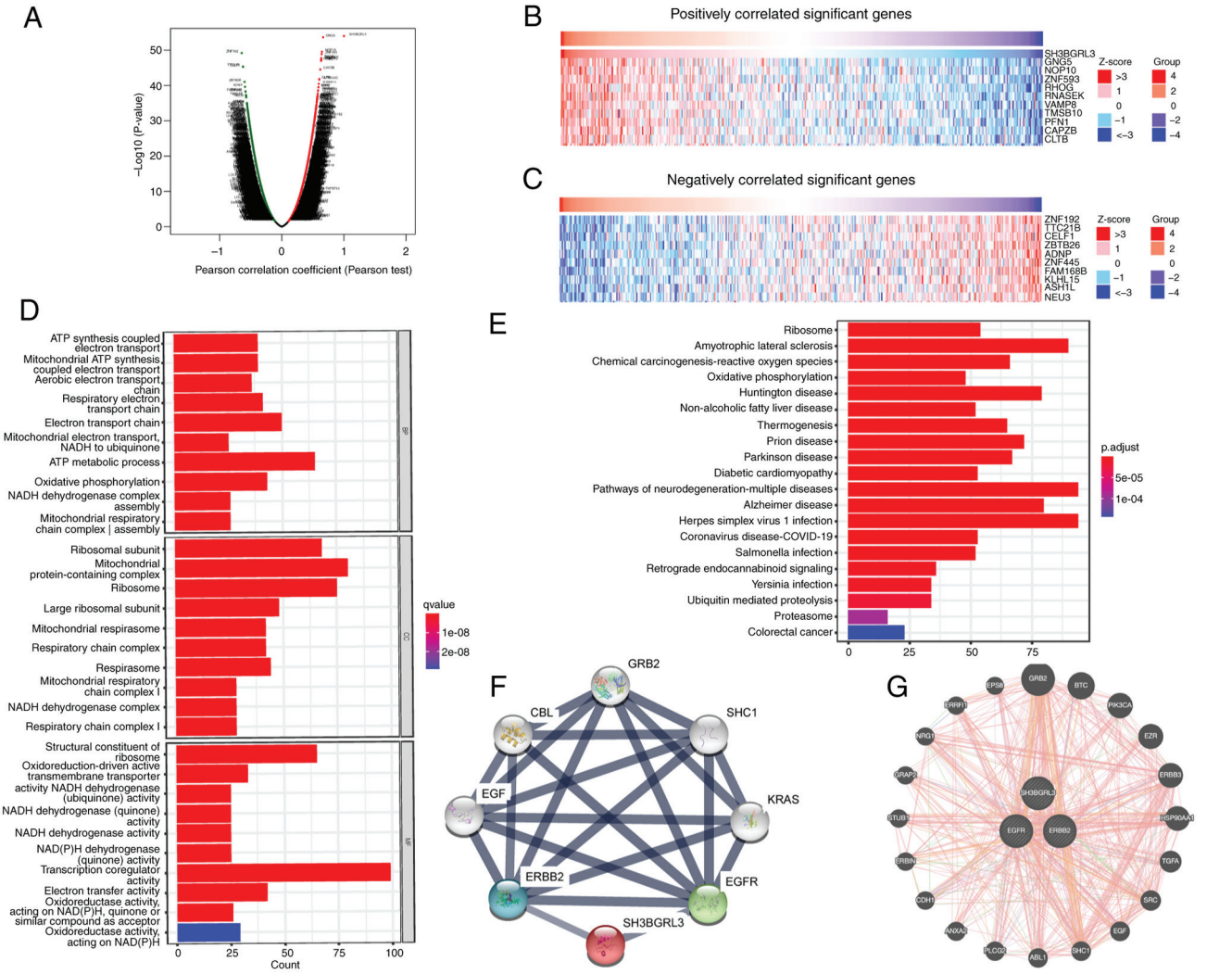


Figure 5. Functional enrichment analysis of SH3BGRL3 and its interactive networks. (A) DEGs of SH3BGRL3 visualized using a volcano map. Top 10 significant (B) positively and (C) negatively related genes shown using a heat map. DEGs of SH3BGRL3 analyzed by (D) Gene Ontology and (E) Kyoto Encyclopedia of Genes and Genomes. Related networks of SH3BGRL3 predicted using (F) Protein-Protein Interaction Networks Functional Enrichment Analysis and (G) GeneMANIA. SH3BGRL3, SH3 domain-binding glutamic acid-rich protein-like 3; DEGs, differentially expressed genes

## Discussion

Although targeted therapies, including anti-HER-2, anti-VEGF and immune checkpoint therapy, hold promise for GC, there is still a lack of effective treatment for most patients in clinical practice. Thus, searching for an alternative prognostic marker and a potential target agent in GC is urgent. The results of the present study indicate that SH3BGRL3 may be an attractive predictive molecule for GC, particularly in EBVnGC. The present study demonstrated that SH3BGRL3 mRNA and protein expression was increased in tumor tissues using data from multiple public datasets and clinical specimens. In GC, especially in EBVnGC, high SH3BGRL3 expression was significantly associated with more aggressive clinicopathological features, such as the presence of perforate serosa, lymph node involvements, cancer embolus and perineural invasion, together with a higher TNM stage. Patients with high SH3BGRL3 expression demonstrated worse outcomes than those with low expression. The findings of the present study indicate that SH3BGRL3 expression could further refine prognosis in patients with GC with the same status of systems such as TNM staging and WHO grading, which could significantly contribute to hierarchical clinical management. Moreover, the nomogram based on SH3BGRL3, preoperative blood glucose and other prognostic variables in EBVnGC in the present study, demonstrated good accuracy and consistency, indicating its predictive value for predicting the prognosis in EBVnGC.

The present study confirmed an association between SH3BGRL3 expression and BUD formation. BUD is usually considered a morphological marker for epithelial-mesenchymal transformation (EMT), which results in cancer invasion and metastasis and has been indicated as an independent adverse prognostic factor for colorectal cancer and other solid tumors, including GC (21). As in previous studies (28,29), the present study demonstrated that BUD was associated with a poor prognosis in patients with EBVnGC. Furthermore, the present study revealed that high BUD was associated with SH3BGRL3 expression. To the best of our knowledge, this is the first study to assess the relationship between SH3BGRL3 expression and BUD. SH3BGRL3 has proline-rich motifs, which could interact with phosphorylated-EGFR through growth factor receptor-bound protein 2 in Akt-related signaling pathways

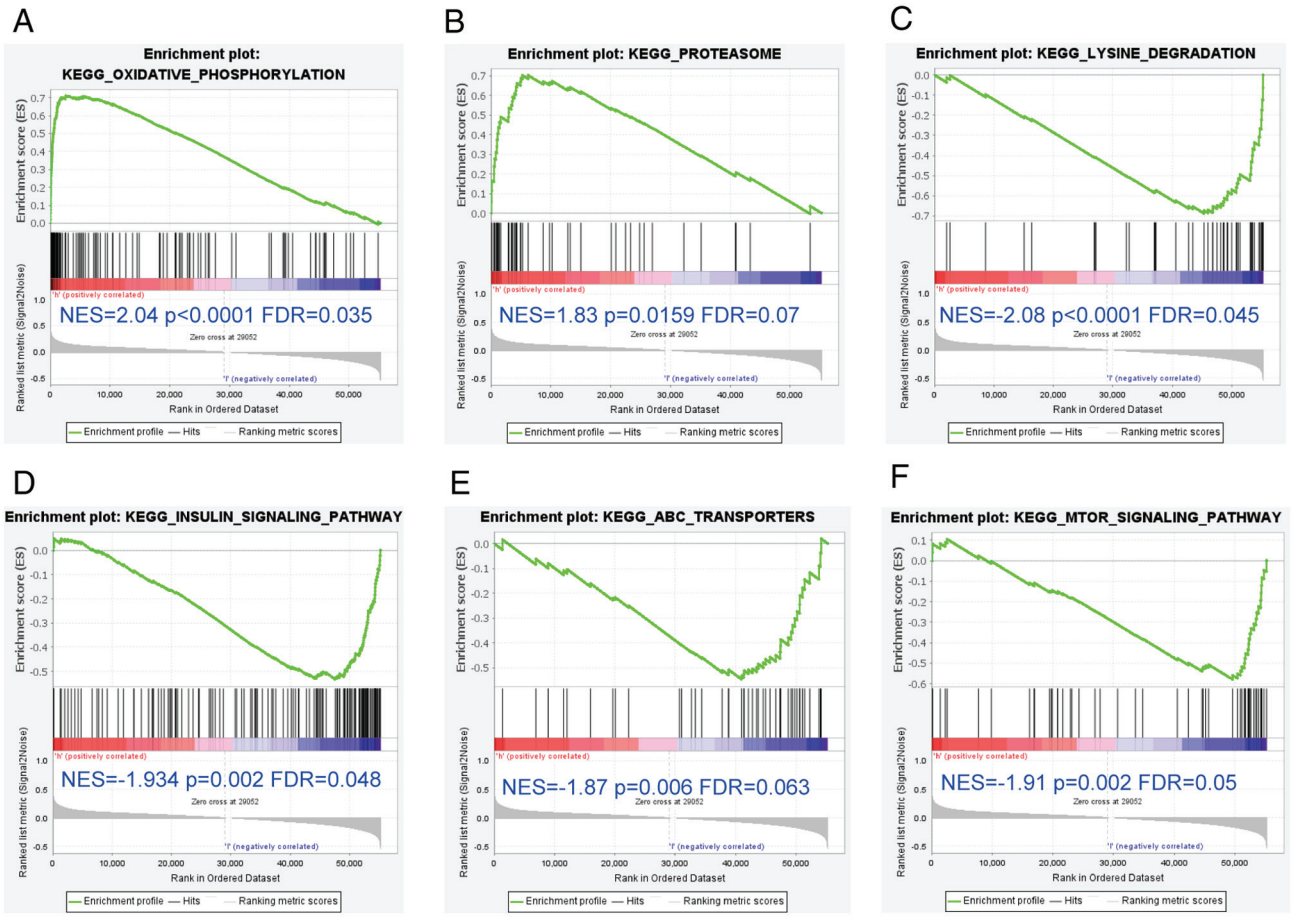


Figure 6. Functional enrichment analysis of SH3BGRL3 in gastric cancer using gene set enrichment analysis. High SH3BGRL3 expression was correlated with gene sets related to (A) oxidative phosphorylation and (B) proteasome pathways, and low SH3BGRL3 expression was correlated with the (C) lysine metabolism pathway, (D) insulin signaling pathway, (E) ABC protein transporters and (F) the mTOR pathway. SH3BGRL3, SH3 domain-binding glutamic acid-rich protein-like 3; ABC, ATP synthase (ATP)-binding cassette; mTOR, Mammalian target of rapamycin.

to promote EMT in tumor cells (11). The two online tools, GeneMANIA and STRING, respectively, predicted that the mRNA and protein expression levels of SH3BGRL3 were associated with ErbB1/EGFR and ErbB2/ERBB2. There was a positive correlation between the expression of ErbB1/EGFR in EBVnGC but not ErbB2/ERBB2, which indicates the potential role of ErbB1/EGFR in cancer progression.

Notably, the results of the present study revealed that SH3BGRL3 expression was significantly associated with preoperative blood glucose levels in EBVnGC. The relationship between blood glucose and GC has been established in previous studies (16,30-32). Hyperglycemia is emerging as a vital factor in the progression of GC, which is considered a cofactor by increasing the risk posed by *H. pylori*-mediated gastric carcinogenesis (30). The present study demonstrated that patients with high blood glucose levels had more adverse outcomes than those without aberrant blood glucose levels in patients with EBVnGC. Furthermore, using KEGG and GO analysis, it was demonstrated that DEGs of SH3BGRL3 were mainly enriched in the regulation of ATP metabolism and synthesis, OXPHOS and the electron transport chain. However, when the data were subdivided into high or low SH3BGRL3 expression, GSEA analysis revealed that the positive regulatory gene sets of OXPHOS were significantly enriched in the high expression group only. In contrast, the insulin and mTOR signaling pathways were significantly enriched in the low expression group, which are classic pathways that involve aerobic glycolysis (33). Aberrant energy metabolism, also called metabolic reprogramming, has been demonstrated in cancer cells for several decades. The Warburg effect indicates that tumor cells could utilize oxygen for aerobic glycolysis to provide energy and meet the requirements for proliferation. It has been previously reported that mitochondrion-mediated OXPHOS is another essential energy source and metabolic precursor for tumor cells by driving ATP synthesis and governing energy metabolism to maintain redox balance. In general, glycolysis and OXPHOS maintain the energy balance in tumor cells (34). However, tumor energy metabolism exhibits more flexibility and extensive heterogeneity. Cancer cells can switch their metabolism from glycolysis to restored suppressed mitochondrial OXPHOS to gain energy, causing hyperglycemia and nutrient shortage (33,35). Recently, studies have reported that enhanced OXPHOS serves essential roles in the malignant development of tumors, including promoting EMT, invasiveness, metastasis, maintaining stem cell properties, and inducing TME remodeling, which may be a potent therapeutic target for advanced solid tumors (34,36,37). The close relationship between SH3BGRL3 and hyperglycemia suggests that SH3BGRL3 may promote glucose metabolism in tumor cells via enhanced OXPHOS, resulting in aggressive

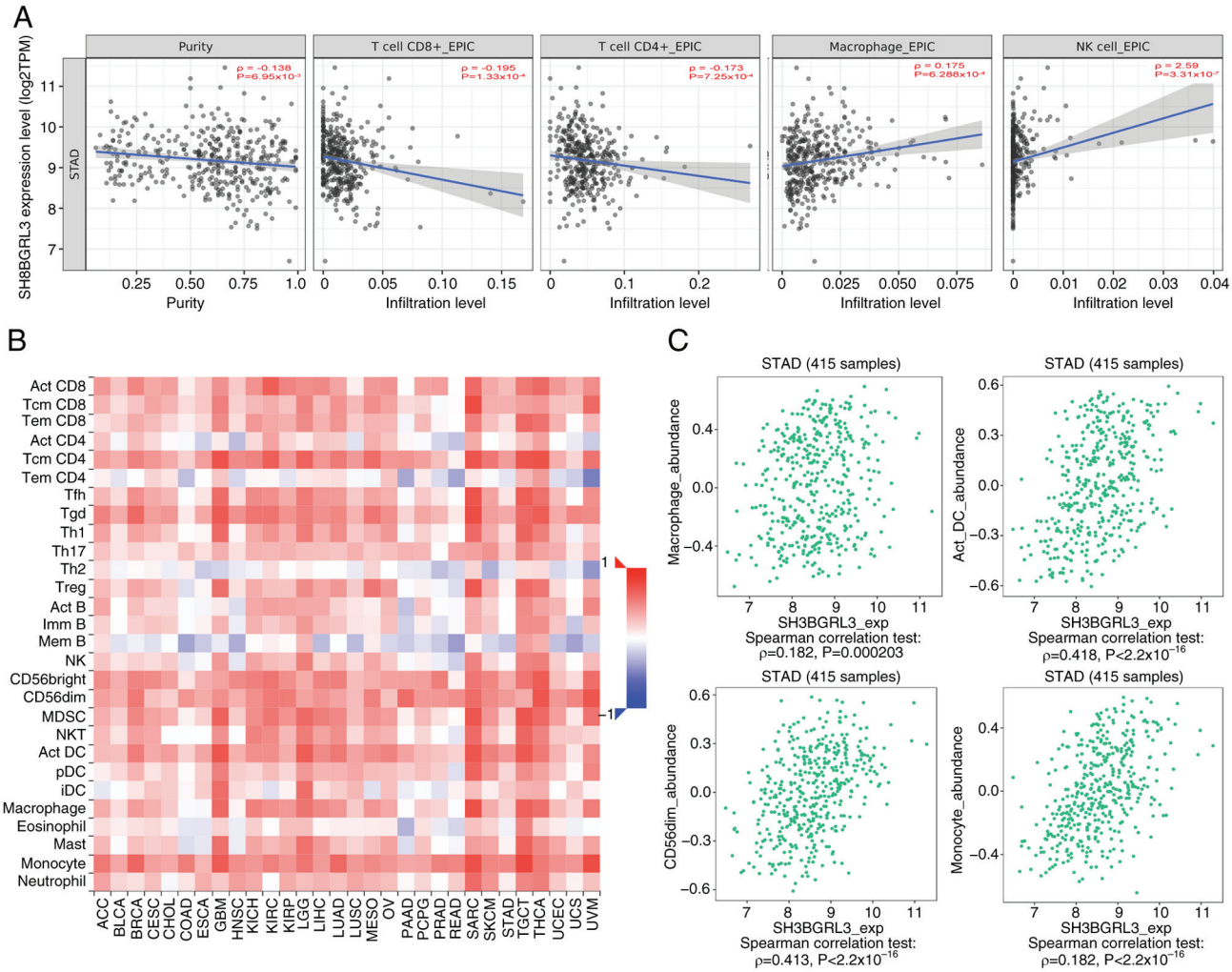


Figure 7. Association between SH3BGRL3 expression level and infiltrating immune cells in gastric cancer from the TIMER and TISIDB databases. (A) TIMER revealed that SH3BGRL3 expression was negatively correlated with $CD4^+$ and $CD8^+$ T, and positively correlated with macrophages and NK cells. TISIDB demonstrated that (B) SH3BGRL3 was associated with infiltrating immune cells within the tumor microenvironment in malignant tumors, including in gastric cancer, and (C) there was a positive correlation between SH3BGRL3 expression and macrophages, dendritic cells, NK $CD56^{dim}$ cells and monocytes. SH3BGRL3, SH3 domain-binding glutamic acid-rich protein-like 3; TIMER, Tumor Immune Estimation Resource; TISIDB, Tumor and Immune System Interaction Database; NK, natural killer; TPM, transcripts per million.

GC phenotypes. The association between SH3BGRL3, glycolysis and OXPHOS may lead to studies on the influence of other metabolic reprogramming processes on EBVnGC transformation and cancer development. Further functional analyses, including the identification of SH3BGRL3 associated glycolysis-associated genes, the investigation of the interaction mechanism between SH3BGRL3 and glycolysis, and the elucidation of the molecular mechanism of SH3BGRL3 involved in regulating the biological behaviors of EBVnGC, are essential areas of future research.

Using two online servers, TIMER and TISIDB, the present study demonstrated that SH3BGRL3 expression was primarily associated with macrophage and NK cell infiltration. In contrast, it was negatively correlated with T lymphocytes within the TME. Macrophages infiltrating malignant tumors are called tumor-associated macrophages (TAMs), which serve a critical role in promoting a suppressive tumor immune microenvironment and escape. TAMs are heterogeneous cells with two dominant populations of classically (M1) and alternatively (M2) activated phenotypes that differ depending on the microenvironmental stimulus (38). Previous studies have reported that TAMs can promote malignant progression involving tumor growth, prognosis and therapeutic resistance in GC (38,39). Furthermore, a meta-analysis demonstrated that the higher quantities of M2 subtypes and total TAMs were both adverse prognostic factors for patients with GC (40). SH3BGRL3 was reported to have a positive association with macrophage aggregation, which may have a positive impact on tumor growth. However, the results of the present study also revealed that SH3BGRL3 expression was positively correlated with NK-$CD56^{dim}$ cells infiltrating in GC, which are innate immune cells and exert an antitumor effect in solid tumors (41). The TME of a solid tumor is complex and highly heterogeneous. The immunosuppressive microenvironment of the tumor could destroy NK cell-mediated immune surveillance, even if NK cells are enriched in abundance (42). Regarding the possible role in regulating metabolic reprogramming, SH3BGRL3 could induce TME remodeling, which may be linked with complex infiltrating immune cells within the GC.

There are certain limitations to the present study. First, although the association between SH3BGRL3 expression and OS in GC and EBVnGC were demonstrated both using public datasets and single-center clinical specimens, further external validation should be performed by multi-center prospective studies. Second, although the relationship between SH3BGRL3 expression and preoperative blood glucose was established and the possible molecular mechanism was explored, further *in vitro* and *in vivo* functional analyses are required to verify the present results in the future.

In summary, the present study demonstrated that SH3BGRL3 is significantly upregulated in GC tissues. Furthermore, SH3BGRL3 is an adverse prognostic factor for GC, particularly in EBVnGC, which could serve as a potential biomarker for patients with GC.

**Acknowledgements**

Not applicable.

**Funding**

The present study was supported by the Startup Fund for Scientific Research, Fujian Medical University (grant no. 2020QH1168), the Natural Science Foundation of Fujian Province (grant no. 2024J011006). the Open Fund from Fujian Key Laboratory of Translational Research in Cancer and Neurodegenerative Diseases (grant no. FKLTR-202101) and Scientific Research Project of the National Key Clinical Specialty Construction Project (grant no. 2022YBL-ZD-05).

**Availability of data and materials**

The data generated in the present study may be from the corresponding author.

**Authors' contributions**

HQL, LYC, XYC and XC conceived and designed the experiments. HQL, LQZ, XBY and XZ performed the experiments. HQL, LQZ and GDZ analyzed the data. HQL, LQZ, XBY, XZ, XYC, LYC and XC provided the reagents, materials and/or the analysis tools. HQL and LYC wrote the paper. HQL, XYC, LYC and XC confirm the authenticity of all the raw data. All authors have read and approved the final manuscript.

**Ethics approval and consent to participate**

The Ethics Committee of Fujian Provincial Hospital (Fuzhou, China) approved the present study with a waiver of informed consent (approval no. K2021-04-094). The present study was performed under the principles of the Declaration of Helsinki.

**Patient consent for publication**

Not applicable.

**Competing interests**

The authors declare that they have no competing interests.

**References**

1. Sung H, Ferlay J, Siegel RL, Laversanne M, Soerjomataram I, Jemal A and Bray F: Global cancer statistics 2020: GLOBOCAN estimates of incidence and mortality worldwide for 36 cancers in 185 countries. CA Cancer J Clin 71: 209-249, 2021.
2. Cancer Genome Atlas Research Network: Comprehensive molecular characterization of gastric adenocarcinoma. Nature 513: 202-209, 2014.
3. Setia N, Agoston AT, Han HS, Mullen JT, Duda DG, Clark JW, Deshpande V, Mino-Kenudson M, Srivastava A, Lennerz JK, *et al*: A protein and mRNA expression-based classification of gastric cancer. Mod Pathol 29: 772-784, 2016.
4. Mazzocco M, Maffei M, Egeo A, Vergano A, Arrigo P, Di Lisi R, Ghiotto F and Scartezzini P: The identification of a novel human homologue of the SH3 binding glutamic acid-rich (SH3BGR) gene establishes a new family of highly conserved small proteins related to thioredoxin superfamily. Gene 291: 233-239, 2002.
5. Berleth ES, Masso-Welch PA, Kazim LA, Ip MM, Mihich E and Ehrke MJ: Expression, tissue distribution, and cellular localization of the antiapoptotic TIP-B1 protein. J Leukoc Biol 69: 995-1005, 2001.
6. Tong F, Zhang M, Guo X, Shi H, Li L, Guan W, Wang H and Yang S: Expression patterns of SH3BGR family members in zebrafish development. Dev Genes Evol 226: 287-295, 2016.
7. Song J and Shen SH: Effects of SH3BGRL3 overexpression on the proliferation and differentiation of human acute promyelocytic leukemia cells. J China Med Univ 48: 338-341, 2019.
8. Lee MJ, Kim J, Kim MY, Bae YS, Ryu SH, Lee TG and Kim JH: Proteomic analysis of tumor necrosis factor-alpha-induced secretome of human adipose tissue-derived mesenchymal stem cells. J Proteome Res 9: 1754-1762, 2010.
9. Jiang M, Lash GE, Zeng S, Liu F, Han M, Long Y, Cai M, Hou H, Ning F, Hu Y and Yang H: Differential expression of serum proteins before 20 weeks gestation in women with hypertensive disorders of pregnancy: A potential role for SH3BGRL3. Placenta 104: 20-30, 2021.
10. Chiang CY, Pan CC, Chang HY, Lai MD, Tzai TS, Tsai YS, Ling P, Liu HS, Lee BF, Cheng HL, *et al*: SH3BGRL3 protein as a potential prognostic biomarker for urothelial carcinoma: A novel binding partner of epidermal growth factor receptor. Clin Cancer Res 21: 5601-5611, 2015.
11. Yin L, Gao S, Shi H, Wang K, Yang H and Peng B: TIP-B1 promotes kidney clear cell carcinoma growth and metastasis via EGFR/AKT signaling. Aging (Albany NY) 11: 7914-7937, 2019.
12. Xiang Z, Huang X, Wang J, Zhang J, Ji J, Yan R, Zhu Z, Cai W and Yu Y: Cross-database analysis reveals sensitive biomarkers for combined therapy for ERBB2+ gastric cancer. Front Pharmacol 9: 861, 2018.
13. Nie Z, Cheng D, Pan C, Wei Z, Wang C and Wang C: SH3BGRL3, transcribed by STAT3, facilitates glioblastoma tumorigenesis by activating STAT3 signaling. Biochem Biophys Res Commun 556: 114-120, 2021.
14. Lega IC and Lipscombe LL: Review: Diabetes, obesity, and cancer-pathophysiology and clinical implications. Endocr Rev 41: bnz014, 2020.
15. Shimoyama S: Diabetes mellitus carries a risk of gastric cancer: A meta-analysis. World J Gastroenterol 19: 6902-6910, 2013.
16. Sheng L, Peng H, Pan Y, Wang C and Zhu Y: Evaluating the effect of diabetes on the prognosis of gastric cancer using a propensity score matching method. J Gastrointest Oncol 11: 999-1008, 2020.
17. Miao ZF, Xu H, Xu YY, Wang ZN, Zhao TT, Song YX and Xu HM: Diabetes mellitus and the risk of gastric cancer: A meta-analysis of cohort studies. Oncotarget 8: 44881-44892, 2017.
18. Faubert B, Solmonson A and DeBerardinis RJ: Metabolic reprogramming and cancer progression. Science 368: eaaw5473, 2020.
19. Zhao L, Liu Y, Zhang S, Wei L, Cheng H, Wang J and Wang J: Impacts and mechanisms of metabolic reprogramming of tumor microenvironment for immunotherapy in gastric cancer. Cell Death Dis 13: 378, 2022.
20. WHO Classification of Tumours Editorial Board. Digestive system tumours: WHO classification of tumours, 5th edition, volume 1. Lyon: IARC, 2019.
21. Lugli A, Kirsch R, Ajioka Y, Bosman F, Cathomas G, Dawson H, El Zimaity H, Fléjou JF, Hansen TP, Hartmann A, *et al*: Recommendations for reporting tumor budding in colorectal cancer based on the international tumor budding consensus conference (ITBCC) 2016. Mod Pathol 30: 1299-1311, 2017.

22. Package Insert, PATHWAY anti-HER-2/NEU (4B5) rabbit monoclonal primary antibody, German, Created: 17.03.2020. Accessed 01.12.2021.
23. Kim CH, Kim SH, Park SY, Yoo J, Kim SK and Kim HK: Identification of EGFR mutations by immunohistochemistry with EGFR mutation-specific antibodies in biopsy and resection specimens from pulmonary adenocarcinoma. Cancer Res Treat 47: 653-660, 2015.
24. Wolff AC, Hammond MEH, Allison KH, Harvey BE, Mangu PB, Bartlett JMS, Bilous M, Ellis IO, Fitzgibbons P, Hanna W, *et al*: Human epidermal growth factor receptor 2 testing in breast cancer: American society of clinical oncology/college of American pathologists clinical practice guideline focused update. J Clin Oncol 36: 2105-2122, 2018.
25. Wang HL, Kim CJ, Koo J, Zhou W, Choi EK, Arcega R, Chen ZE, Wang H, Zhang L and Lin F: Practical immunohistochemistry in neoplastic pathology of the gastrointestinal tract, liver, biliary tract, and pancreas. Arch Pathol Lab Med 141: 1155-1180, 2017.
26. Ikeda T, Gion Y, Sakamoto M, Tachibana T, Nishikori A, Nishimura MF, Yoshino T and Sato Y: Clinicopathological analysis of 34 Japanese patients with EBV-positive mucocutaneous ulcer. Mod Pathol 33: 2437-2448, 2020.
27. Livak KJ and Schmittgen TD: Analysis of relative gene expression data using real-time quantitative PCR and the 2(-Delta Delta C(T)) method. Methods 25: 402-408, 2001.
28. Kemi N, Eskuri M, Ikäläinen J, Karttunen TJ and Kauppila JH: Tumor budding and prognosis in gastric adenocarcinoma. Am J Surg Pathol 43: 229-234, 2019.
29. Ulase D, Heckl S, Behrens HM, Krüger S and Röcken C: Prognostic significance of tumour budding assessed in gastric carcinoma according to the criteria of the international tumour budding consensus conference. Histopathology 76: 433-446, 2020.
30. Yang HJ, Kang D, Chang Y, Ahn J, Ryu S, Cho J, Guallar E and Sohn CI: Diabetes mellitus is associated with an increased risk of gastric cancer: A cohort study. Gastric Cancer 23: 382-390, 2020.
31. Kim YM, Kim JH, Park JS, Baik SJ, Chun J, Youn YH and Park H: Association between triglyceride-glucose index and gastric carcinogenesis: A health checkup cohort study. Gastric Cancer 25: 33-41, 2022.
32. Karlin NJ, Buras MR, Kosiorek HE, Verona PM and Cook CB: Glycemic control and survival of patients with coexisting diabetes mellitus and gastric or esophageal cancer. Future Sci OA 5: FSO397, 2019.
33. Yuan LW, Yamashita H and Seto Y: Glucose metabolism in gastric cancer: The cutting-edge. World J Gastroenterol 22: 2046-2059, 2016.
34. Hu Y, Xu W, Zeng H, He Z, Lu X, Zuo D, Qin G and Chen W: OXPHOS-dependent metabolic reprogramming prompts metastatic potential of breast cancer cells under osteogenic differentiation. Br J Cancer 123: 1644-1655, 2020.
35. Thankamony AP, Saxena K, Murali R, Jolly MK and Nair R: Cancer stem cell plasticity-a deadly deal. Front Mol Biosci 7: 79, 2020.
36. Kalyanaraman B, Cheng G and Hardy M: Therapeutic targeting of tumor cells and tumor immune microenvironment vulnerabilities. Front Oncol 12: 816504, 2022.
37. Janku F, Beom SH, Moon YW, Kim TW, Shin YG, Yim DS, Kim GM, Kim HS, Kim SY, Cheong JH, *et al*: First-in-human study of IM156, a novel potent biguanide oxidative phosphorylation (OXPHOS) inhibitor, in patients with advanced solid tumors. Invest New Drugs 40: 1001-1010, 2022.
38. Ruffell B and Coussens LM: Macrophages and therapeutic resistance in cancer. Cancer Cell 27: 462-472, 2015.
39. Gambardella V, Castillo J, Tarazona N, Gimeno-Valiente F, Martínez-Ciarpaglini C, Cabeza-Segura M, Roselló S, Roda D, Huerta M, Cervantes A and Fleitas T: The role of tumor-associated macrophages in gastric cancer development and their potential as a therapeutic target. Cancer Treat Rev 86: 102015, 2020.
40. Wang XL, Jiang JT and Wu CP: Prognostic significance of tumor-associated macrophage infiltration in gastric cancer: A meta-analysis. Genet Mol Res 15: gmr15049040, 2016.
41. Oya Y, Hayakawa Y and Koike K: Tumor microenvironment in gastric cancers. Cancer Sci 111: 2696-2707, 2020.
42. Mylod E, Lysaght J and Conroy MJ: Natural killer cell therapy: A new frontier for obesity-associated cancer. Cancer Lett 535: 215620, 2022.